CHAPTER V

THEORY OF COARSENING

The range of model types that have been used to simulate grain growth is extremely large. Broad categories include pure phenomenological models, pure statistical models, mean field theories, "exact" vertex and boundary evolution models, and Potts model simulations. All have been successful to varying degrees. An important division exists between models that attempt to predict equilibrium distribution functions based on purely statistical or geometrical considerations and dynamical models which focus primarily on grain growth rates, though they may supply information on distribution functions as well. We will first examine static models and then move on to the many categories of dynamic simulation.

V.a Static Models

The construction of pure geometric models based on random partitions of the plane, and attempts to determine their properties analytically, have amused geometers for at least two hundred years.[34,52,90,164,245] The elegance of some of the solutions and the complicated analytic geometry of others is impressive in its own right, but these models also have some claim to be considered as models for grain growth (in the case of nucleation they can work very well). In addition, the exact solutions of the properties of these models provide an extremely useful baseline for comparison to experiment and less rigorous simulations. Especially for the Voronoi type models there are

many analytic results for area and side distributions and correlations which are difficult or impossible to obtain for more complicated constructions.[164] Perhaps, the simplest approach to modeling the soap froth is to examine the statistical properties of its long term state considered as a fixed polygonal lattice. Taking this idea to an extreme we might study the regular hexagonal honeycomb as a model of the froth. Such a model is not very useful for studies of coarsening, but as we noted above, it gives useful results in studies of foam rheology.

V.a.i Voronoi Type Models

Slightly more realistic models must take into account the fundamental disorder of the froth and attempt to duplicate it geometrically. Most simply we may throw down a set of points at random locations with some average density, and assign to each point that subset of the plane which is closer to it than to any other point, a process known as the **Voronoi Construction** (see Fig. 27 (A)).[34,52,88,89,90,151,245,254] This construction subdivides the plane into a unique network of polygons with straight sides and vertices with coördination number three, but with a range of vertex angles and a very broad area distribution. In nucleation, this model corresponds to throwing down a set of nucleation centers at a fixed time and growing a circular domain from each at a fixed rate. The area distributions can be regularized by establishing an excluded volume during seeding, so that the initial particles are separated by a minimum distance (see Fig. 24 (A)). This narrows both the area and number-of-sides distributions, and results in angles more nearly

Fig. 19 Glass Models. (A) Triangle raft. (B) Triangle-Line raft (From Shackelford 1982).[204]

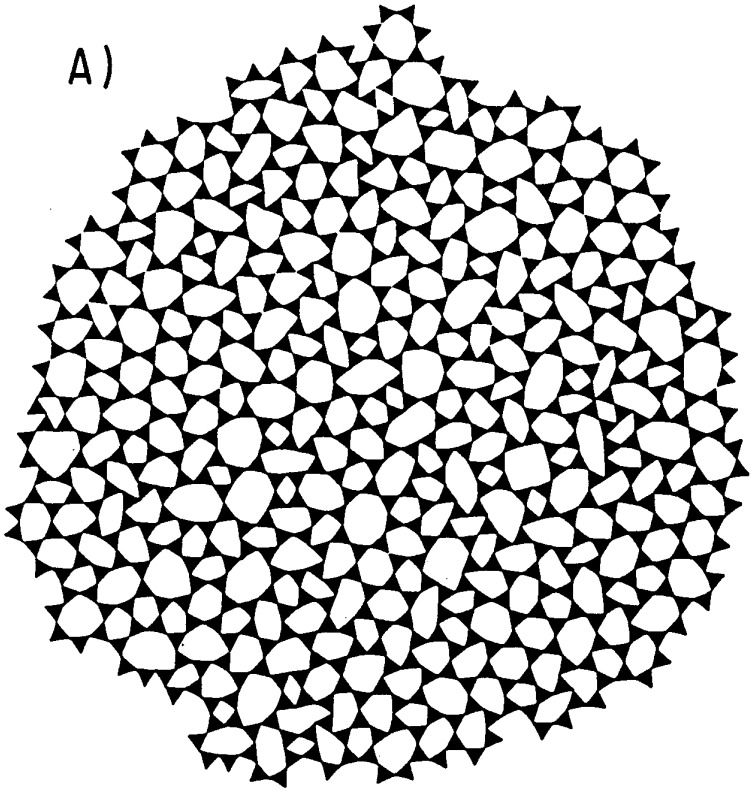
A)

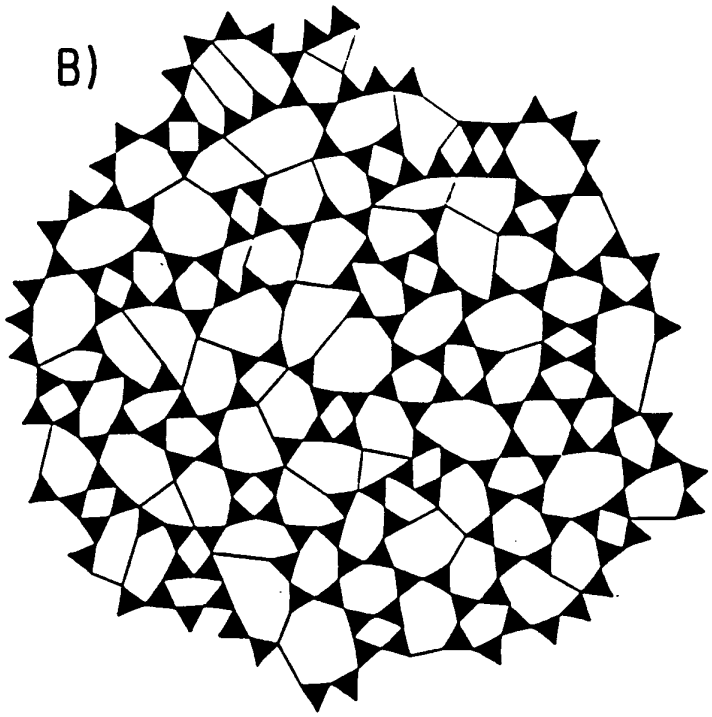
B)

Fig. 20 Dual Lattice. Sample of a two dimensional soap froth (solid lines) with the triangular dual lattice (dashed lines) indicated. Points replace bubbles, and dashed lines between points replace edges between neighbors (From Kikuchi 1956).[121]

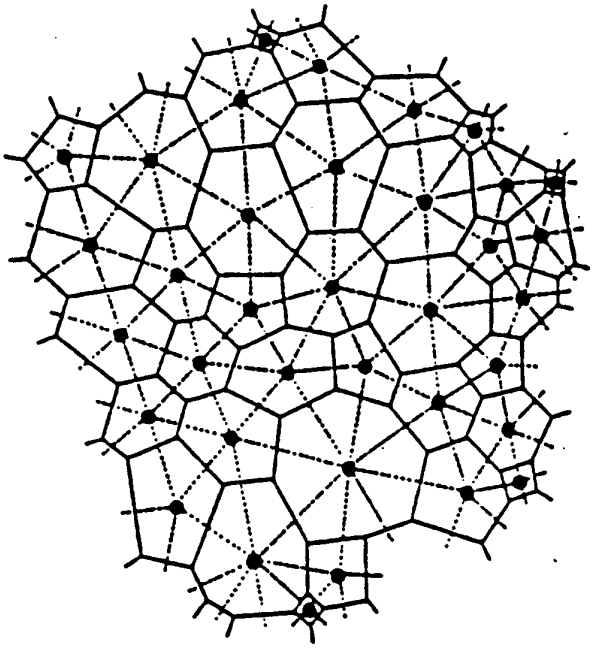

120°. The resulting pattern looks more like a real froth but still has non-120° angles and too narrow a side distribution.[80]

The fundamental problem with models of this sort is that they freeze in large scale inhomogeneities present in the seed pattern which would be rapidly relaxed in a real froth. We can approximate this relaxation geometrically by iteratively performing the Voronoi construction and moving each nucleation center to a new position at the center of its polygon until we reach an invariant pattern. This is known as a relaxed Voronoi construction.[105]

A third approach is to seed continuously but randomly in time in the "uncrystallized area" while growing uniformly (the **Johnson-Mehl model**), again producing a more irregular pattern than that observed in experiments, but which can be regularized using an excluded volume or relaxation.[164] Frost and Thompson have studied extensively,[80] the effects of changing the rates and types of nucleation and relaxation on the final distributions. In no case do they find the observed experimental dominance of five-sided bubbles, but the range of distributions they obtain is impressive.

One place where Voronoi networks are useful is to generate initial conditions for simulations. In this case, any initial stresses equilibrate quickly, and the patterns are sufficiently random to converge rapidly to a scaling state. Both Frost and Thompson and Anderson *et al.* have discussed the consequences of the choice of initial conditions.[80,15]

An additional application of the Voronoi construction in two dimensions is to determine adjacencies when the widths of the boundaries between

bubbles are comparable to the bubble size as happens in magnetic and lipid monolayer froths. In this case the Voronoi construction applied starting with the centers of each bubble, gives a unique assignment of areas and neighbors.

We also mention briefly a class of glass models originally proposed by Zachariasen.[204,256,258] We place equilateral triangles successively with vertices touching and without overlap, in a clockwise spiral around a seed triangle. At each step we randomly choose a number between four and eight and attempt to build a closed ring with that number of links. Since not all target rings sizes are possible at any given time we obtain a nontrivial side distribution function for the number of triangles per ring (See Tables 7 and 8 and Fig. 19 (A)). Shackelford also proposed an extended model which gave a narrower side distribution by allowing the use of lines as well as triangles, a line being inserted if it would a) close a loop with six or more triangles which had its target number of sides or more, and b) have a length between one and two times the length of a triangle edge (See Tables 7 and 8 and Fig. 19 (B)).

V.a.ii Maximum Entropy Models

We may extend our geometrical models a little more (as we did by introducing relaxation), by considering the final distribution to be the limit of a repetitively applied geometrical process. Kikuchi looked for the most probable network configuration based on independent weighting of configurations in the dual lattice (the pure triangular lattice obtained by replacing each bubble by a point at its center, and each edge by a line connecting

the centers of the neighbors (See Fig. 20).[121] In his first model (Kikuchi I) he assumed that the bubble centers lay on a regular triangular lattice and calculated the relative frequency of nearest neighbor and next nearest neighbor links which gave the largest number of possible configurations, i.e. the highest entropy. Then he calculated the distribution functions for this most probable state. In his second model (Kikuchi II) he allowed vacancies in his triangular lattice and third nearest neighbor links, again calculating the most probable state and its distribution functions (See Tables 7 and 8). Weaire has used a similar argument employing the probabilities of various topological transforms on a lattice to obtain the nearest neighbor number of sides correlation for an equilibrated froth (See Table 11).[134,135]

We can be slightly more sophisticated and try to guess the constraints on a topological lattice. If the constraints are correctly chosen, then in statistical equilibrium, the actual distribution functions should be such as to maximize the distribution function's entropy subject to those constraints, for example the first three or four moments of the distribution functions.[50,115,116,139] The difficulty in this "Maximum Entropy" method is to choose the constraints correctly.

Rivier has championed maximum entropy models and done extensive analyses to predict the soap froth's distribution functions.[199] He solves the joint distribution function $\rho(n, A)$ to maximize the entropy,

$$S \equiv -\sum_{n,A} \rho(n, A) \log(\rho(n, A)) \qquad \text{(V.1)}$$

subject to the constraints that $< n >= 6$, that $< a >$ is known, and that that either Lewis' law for areas, $< A_n > \propto n$, or the radius law, $< r_n > \propto n$ (where $< r_n >$ is the average radius of an n-sided bubble) applies. The two predictions of interest are that the area distribution function will decay exponentially,

$$\rho(A) \propto \exp^{-\lambda_1 A}, \tag{V.2}$$

where λ_1 is a fitting parameter, or, defining $a' \equiv \log(\frac{A}{<a>})$,

$$\rho(a') = \log(a') \exp^{-a'}. \tag{V.3}$$

The number of sides distribution takes the form

$$\rho(n) = \epsilon(n - c_1) \exp^{-\gamma n}, \tag{V.4}$$

where γ and ϵ are fitting parameters, and c_1 is a constant taken from Lewis' Law (described in section VII.a).

Almeida and Iglesias have done the same thing adding a bulk energy, proportional to bubble area.[10] This has the peculiar effect of making $< a_n >$ roll over rapidly in n so that many-sided bubbles all have the same area, and $\rho(n)$ is monotonically decreasing in n. A later paper by the same authors instead assumes that the average side length of bubbles is uniform and, taking the second moment of the side distribution as a parameter, obtains acceptable results for $\rho(n)$ and $< a_n >$ (See Tables 7, 8 and 11).[11]

V.b A Phenomenological Model

Another approach is to discard microscopic considerations entirely and to try to model the disordering process directly, considering only its salient physical features. Such an approach cannot hope to predict the growth exponent in the scaling regime, but it can provide a check on how well we understand the froth's approach to equilibrium. Based on the observations that disordered regions eat away at islands of hexagons from the edges, and that the long term rate of area growth is a power law in time, Glazier, Gross and Stavans wrote the following phenomenological model.[94]

They divided the population of bubbles into two classes, the bubbles in ordered regions and the bubbles in disordered regions, denoting the number of bubbles in each class by $O(t)$ and $D(t)$ respectively, with the total number of bubbles, $N(t) \equiv O(t) + D(t)$. They next assumed that ordered bubbles did not evolve but were converted into disordered bubbles at a rate proportional to the total contact area between order and disorder (making use of the experimental observation that ordered patches were stable except where they were eaten away by disorder from their edges). To lowest order, assuming random distributions, contact area is proportional to $\frac{O(t) \cdot D(t)}{O(t)+D(t)}$ which implies:

$$\frac{dO(t)}{dt} = -\kappa_1 \frac{O(t) \cdot D(t)}{O(t) + D(t)} \tag{V.5}$$

where κ_1 is a constant to be determined and represents the rate at which disorder diffuses into ordered patches.

They also assumed that the rate of disappearance of bubbles in disordered regions was independent of $O(t)$ and was uniform in t, since experimentally

they obtained nearly power law behavior for the area atlong times, when the system appeared completely disordered, i.e., $N(t) \propto t^{-\alpha}$. These assumptions yield an equation for $D(t)$ including terms for the conversion of order to disorder and for power law dissipation:

$$\frac{dD(t)}{dt} = \kappa_1 \frac{O(t) \cdot D(t)}{O(t) + D(t)} - \kappa_2 D(t)^{\beta}, \tag{V.6}$$

where $\alpha = \frac{1}{\beta - 1}$. While both $O(t)$ and $D(t)$ are abstract quantities, since $O(t)$ in particular is not simple to measure (there are six-sided bubbles in disordered regions as well as ordered regions), combining them produces a quantitative measure of the system disorder which we can then compare to other possible measures, the **Disorder**

$$\partial \equiv \frac{D(t)}{O(t) + D(t)}. \tag{V.7}$$

The parameter ∂ runs from zero for a perfect hexagonal lattice, to one for an equilibrated froth in a power law scaling state. Thus its time evolution provides information about the transition from order to disorder. It has significant advantages over most other measures of disorder since it can be computed from $N(t)$ directly without calculating the distribution functions. It is also an intrinsically averaged quantity, much less sensitive to small fluctuations than high order moments and therefore is usable in smaller scale systems. Glazier, Gross and Stavans calculated ∂ by fitting $N(0)$, β, κ_1, κ_2 and $\partial(0)$ to give a minimal least squares error against the experimental $N(t)$, but β, κ_2 and $N(0)$ can all be measured independently.

We present Glazier, Gross and Stavans' values for ∂ in Fig. 16 (dashed lines). For initially ordered runs, Fig. 16 (a)-(e), ∂ behaved as expected,

increasing smoothly to 1, and reaching its final value where the experimental value of $N(t)$ rolled over into a power law. For the initially disordered run shown in Fig. 16 (f), the rate of conversion from order to disorder was slower than the rate of loss of disorder, and ∂ decreased slightly before increasing to one at the rollover. While Glazier, Gross and Stavans originally dismissed this decrease as an artifact of the model, Stavans and Glazier have since shown that it accurately reflects the disordering of the pattern.[220] We will return to this point in our discussion of the moments of the distribution functions. As expected, ∂ was small for apparently well ordered conditions, e.g. $\frac{\rho(5)}{\rho(6)} < 0.1$ and large for disordered conditions, e.g. $\frac{\rho(5)}{\rho(6)} > 1.0$.

In Fig. 16 we also show Glazier, Gross and Stavans' fits for $N(t)$ (solid lines). The fits yielded a value of $\beta = 2.7 \pm 0.3$ corresponding to $\alpha = 0.59(^{+0.11}_{-0.09})$. We believe that their error estimate was rather optimistic because of the systematic boundary effects we have discussed, but it did accurately reflect the numerical range in the estimate of the exponent. The typical error of their fits for $N(t)$ was better than 3%, and the maximum observed error was 5%. In the two runs with the most complete time series, Fig. 16 (d) and Fig. 16 (f), the apparent power law behavior held over a full decade, so the deviation in exponent from $\alpha = 1$ was not due simply to noisy measurements. The excellent quantitative agreement between the behavior of the model and the experiment, with a perfect matching of the transient over a wide range of initial disorders strongly suggests that the model contains most of the essential physics of the transition.

V.c Radius Based Mean Field Theories

The term mean field theory is a broad one and we will discuss three separate categories, roughly in their historical order of development: dynamic theories based solely on the distribution of grain radii, theories based on both area and side distributions, and semi-exact models which keep track of the structure of the topological network defined by the dual lattice. In our discussion we will examine the predicted growth exponents and ability to duplicate transients as indicators of the reasonableness of the theory.

Many of the models we present in this section emphasize simplicity at the expense of much of the basic physics of grain growth. Historically, part of the difficulty developing an adequate theory of coarsening was the focus on grain growth in metals, in which it was impossible to measure the key parameter, namely how the growth rate of a grain depended on its size and geometry. It was therefore a common practice to start with an experimental result (like a distribution function) and to work backwards to determine the basic dynamical laws. In the absence of experimental checks on the dynamics this procedure allowed essentially any result to be obtained. Another result of the focus on metals was a general neglect of geometrical factors which were hard to measure. Models tended to assume the proverbial spherical cow, neglecting transients and equilibration processes, and frequently, for good measure, invoking log-normal area distributions. Since von Neumann showed that it is the number of sides a grain has and not its size that determines the grain's growth rate, it is somewhat surprising that radius

based models work at all. What saves them is the strong correlation between number of sides and grain (or bubble) area. One decided advantage of radius based models is that they are independent of dimension, giving useful results for bulk grain growth, when the absence of an equivalent to von Neumann's law in three dimensions makes it difficult to develop more sophisticated models. Additionally the success of radius based theories in explaining Ostwald ripening (the growth of widely separated grains interacting with a gas) suggests that these theories may be more relevant to the case of liquid-gas phase transitions than they are to coarsening of froths.[117,231]

In our discussion we will consider only the mathematical formalism of these theories, not the elaborate attempts to evaluate the various physical parameters such as activation and surface energies and temperature dependencies, which were of specific interest in metallurgical applications.

V.c.i Burke and Turnbull: a Zeroth Order Model

In a long review, primarily concerned with microscopic properties of metal grains, Burke and Turnbull,[42] discussed the coarsening dynamics of metal grains, drawing a specific analogy to the evolution of a soap froth. Their analysis neglected all interactions between grains which they considered as circular or spherical, so it certainly qualifies as a mean field theory. They assumed, based on both microscopic energy considerations and surface tension arguments, that for any grain, the rate of boundary migration was,

$$v = \mu\sigma\frac{V}{\rho}, \tag{V.8}$$

where μ is a temperature dependent mobility, σ a surface energy, ρ the integrated radius of curvature, and V the atomic volume. This is just a scalar form of equation (III.8). Assuming that all these constants were indeed constant, that the radius of curvature was proportional to the grain radius, r, and that the change in average grain diameter was proportional to the rate of boundary migration, they obtained

$$\frac{dr}{dt} = \frac{\kappa}{r}, \tag{V.9}$$

where κ is a diffusion constant. Integrating this differential equation (which is essentially equivalent to the second term in the phenomenological model presented previously), produced

$$< a(t) >= \sqrt{\kappa t + a_0}. \tag{V.10}$$

So for long times $\alpha = 1$. The analysis is completely independent of whether the grain growth occurs in two or three dimensions. Burke and Turnbull noted agreement with scaling measurements in a two dimensional soap froth by Fullman,[86] and rather optimistically concluded "The fact that $< r > \propto t^{1/2}$ indicates that the geometrical analysis is essentially correct." They then suggested several mechanisms to explain the observed deviations from this scaling law in real metal systems. Unfortunately, as shown in the section on von Neumann's law, any mean field theory must yield a long term scaling exponent of one, so the agreement with experiment was fortuitous.[173,174]

Rhines and Craig took a view similar to that presented in the phenomenological model above,[194] looking at coarsening as the progressive elimination

of individual grains with average area $< a >$. They derived the dynamics of their equation by assuming a bubble like diffusive motion of grain boundaries,

$$v = \mu \Delta P = \mu(\frac{1}{\rho_1} + \frac{1}{\rho_2}), \tag{V.11}$$

which meant that the change in volume per unit time of a grain was

$$\frac{dV}{dt} = \mu M S, \tag{V.12}$$

where, M is the grain's integrated curvature and S the grain's surface area. They next cited as an experimental fact that the product, $MS = \Sigma$, was proportional to the length scale in any given experiment, and defined a **sweep constant**, Θ, the number of grains lost per unit distance of boundary motion. There has been some debate as to whether this choice of sweep constant was correct, but for our purpose we need only note that in a scaling state it must scale inversely with length scale.[58,111,195] Swallowing Θ, μ and Σ into a single rate constant κ they concluded that the number of grains in a given volume goes as

$$\frac{d}{dt}\frac{1}{N} = \frac{1}{N_0}(1 + \kappa), \tag{V.13}$$

putting in the initial condition $N(0) = N_0$. Again we obtain $\alpha = 1$ at long times in three dimensions.

V.c.ii Diffusional Radial Mean Field Theories

The most obvious defect with the Burke and Turnbull and Rhines and Craig models is their inability to predict radius or area distribution functions. Several authors have proposed models which address directly the mean field

evolution of the area distribution. The basic formalism of these models is the same. Consider the distribution function of radii, $\rho(r)$. The evolution of this function may be described in terms of a probability current,

$$j(r) = -D\frac{\partial \rho(r)}{\partial r} + \rho(r)v(r), \tag{V.14}$$

where the first term describes diffusional processes tending to broaden the distribution function and the second deterministic evolution, D being a diffusion constant and $v(r)$ the growth rate as a function of radius. As we shall see later, when applied to a distribution function including number of sides as well as areas, this probability current formalism is completely appropriate to a correct mean field theory of froth coarsening. The difficulty in this case is that there is no simple way to reduce diffusion in the number of sides distribution to diffusion in area distribution. Assuming the appropriateness of this current, the continuity equation gives the time evolution of the distribution as:

$$\frac{\partial \rho(r)}{\partial t} = -\frac{\partial j(r)}{\partial r} = \frac{\partial}{\partial r}(D\frac{\partial \rho(r)}{\partial r}) - \frac{\partial}{\partial r}(\rho(r)v(r)). \tag{V.15}$$

We are now free to speculate on various values for D and $v(r)$. We note that this is the basic structure of the famous Lifschitz-Slyozov model for Ostwald ripening.[148,149]

V.c.iii Deterministic Models

We first consider models that neglect the diffusive term in the evolution equation (i.e. set $D = 0$). In essence these models neglect the possibility that a grain can gain or lose sides in time. One can either hypothesize a form for

$v(r)$ and solve for the area distribution or vice versa. Feltham hypothesized a log normal limiting distribution of areas

$$\rho(r) = \frac{1}{r}\exp\{-|\frac{1}{k_2}\ln\frac{r}{<r>}|^2\} \tag{V.16}$$

and applied an areal approximation to von Neumann's law to obtain the result that for a given grain:

$$\frac{dr^2}{dt} = \kappa\ln(\frac{r}{<r>}). \tag{V.17}$$

Assuming self similar distributions, he then obtained the unsurprising result that $< a > \propto t$.[64] Hunderi and Ryum solved $v(r)$ for several different proposed area distributions.[112,113,114]

Hillert began with our equation (III.8), assuming the basic relation that interface velocity is proportional to the curvature driven pressure difference:[106]

$$v = \mu\Delta P = \mu\sigma(\frac{1}{\rho_1} + \frac{1}{\rho_2}), \tag{V.18}$$

where the ρ_i are the principle radii of curvature. He then assumed that small grains shrink and large grains grow. Since many sided grains tend to be large this was not too unreasonable an assumption. In this case he proposed a specific relation between grain curvature and grain size, of

$$v(r) \propto (\frac{1}{r_{crit}} - \frac{1}{r}), \tag{V.19}$$

where r_{crit} is the average radius of a grain in two dimensions (derived by working backwards from von Neumann's Law!) and an experimentally determined parameter in three dimensions. Substituting he obtained

$$\frac{dr}{dt} = \kappa(\frac{1}{r_{crit}} - \frac{1}{r}), \tag{V.20}$$

which, assuming equilibrated distribution functions yielded the expected $< a > \propto t$. He also made a detailed prediction for the area distributions using the Lifschitz-Slyozov method. Letting $r' \equiv \frac{r}{r_{crit}}$ he found

$$\rho(r') = (2e)^{\delta} \cdot \frac{\delta r'}{(2-r')^{2+\delta}} \cdot \exp \frac{-2\delta}{2-r'}, \tag{V.21}$$

where δ is the dimension.

Kirchner has applied a similar argument to obtain the size distribution function for lens shaped (two-sided) grains growing in grain boundaries.[122] Thompson has also extended the model to include anisotropy and pinning effects to study the growth of free grains in a medium.[227]

Hunderi and Ryum set up a radius based model of this sort in three dimensions, which explicitly considered grain-grain interactions.[112,114] where

$$\frac{dr_i}{dt} = -\frac{\kappa}{{r_i}^2} \sum_{\substack{neighbors \\ j}} A_{ij}(\frac{1}{r_i} - \frac{1}{r_j}), \tag{V.22}$$

where $A_{ij} \equiv \pi \min({r_i}^2, {r_j}^2)$ is the contact area between grains. They assigned grain contacts by position in the index list rather than by looking at a network topology, so this is a pure mean field theory rather than a network model. In their first paper they obtained a scaling exponent of $\alpha = 1$ but later revised their figure to $\alpha = 0.76 \pm 0.04$.

Novikov produced a closely related interaction model.[183] He discretized the radius distributions (bin width Δ, $r_i = \Delta \cdot i$, $N_i \equiv$number of grains in bin i), and assumed completely random attachments and constant grain

boundary mobility. As before

$$\Delta P_{ij} = 2\sigma(\frac{1}{\rho_j} - \frac{1}{\rho_i}). \tag{V.23}$$

However, he used a different, nonsymmetric contact area:

$$A_{ij} = \frac{{r_j}^2}{4(r_i + r_j)^2}. \tag{V.24}$$

So the change in radius from any one contact between class i and class j was:

$$\frac{dr_i}{dt} = 2\sigma \frac{{r_j}^2}{4(r_i + r_j)^2}(\frac{1}{\rho_j} - \frac{1}{\rho_i}). \tag{V.25}$$

As in the phenomenological model, the number of contacts between class i and class j is

$$N_i{}^j = k_i \frac{N_i N_j}{N}, \tag{V.26}$$

where k_i is a normalization to make the total areas come out consistent. This yields

$$\frac{dN_i{}^j}{dt} = \frac{k_v}{8} N_i{}^j \frac{dr_j}{dt}, \tag{V.27}$$

where k_v is the averaged renormalization constant. Finally, summing over classes, yields a master equation:

$$\frac{dN_i}{dt} = -\sum_{j=1}^{i-1} \frac{dN_i{}^j}{dt} + \sum_{j=1}^{i-2} \frac{dN_{i-1}{}^j}{dt} \tag{V.28}$$

$$-[outscatter\ down] + [inscatter\ up]$$

$$-\sum_{j=i+1}^{i_{max}} \frac{dN_i{}^j}{dt} + \sum_{j=i+2}^{i_{max}} \frac{dN_{i+1}{}^j}{dt}$$

$$-[outscatter\ up] + [inscatter\ down].$$

Novikov solved the master equation using a montecarlo method and deleting downscattered grains in class 1. Depending on the absolute length scale of his initial conditions he obtained either $\alpha = 0.792 \pm 0.016$ or $\alpha = 0.720 \pm 0.01$, suggesting some problems in reaching complete convergence. Using the same model with two values of grain boundary mobility he has measured the distribution functions and exponents for anomalous grain growth, and he has also studied boundary pinning using a damped equation for boundary motion:

$$\frac{dr_i}{dt} = 2\sigma(\frac{1}{\rho_j} - \frac{1}{\rho_i} - F), \tag{V.29}$$

where F is a pinning force.[184]

Abbruzzese and Lücke have examined the effects of defect pinning[2,5] and anisotropy[4] on models of this type. For normal grain growth they have compared the theoretical predictions for experimental values obtained in thin sheets of iron alloy, with reasonable success.

Beenakker has also written a radius based mean field theory, which began with von Neumann's law,[25] but then made an *ad hoc* assumption that the free energies of individual grains were minimized, resulting in a nonlinearly increasing dependence of $< a_n >$ on n. The model has the peculiar property that the area distribution broadens to a width of 3.2 and then narrows again to a width of 0.25. The long term growth exponent is $\alpha = 1$.

V.c.iv Diffusive Models

An alternative approach is due to Louat, whose two dimensional analysis

began by noticing that von Neumann's law held only on average experimentally.[152] He proposed that the rate of side swapping could be regarded as so large that the von Neumann's law component of the distribution function evolution could be completely neglected. He therefore wrote the basic evolution equation as:

$$\frac{\partial \rho(r)}{\partial t} = D\frac{\partial^2 \rho(r)}{\partial r^2}. \tag{V.30}$$

Assuming that there are no zero sized or infinite sized grains, the resulting evolution is:

$$\rho(r,t) = cr \exp\left(\frac{-r^2/4Dt}{Dt^{3/2}}\right), \tag{V.31}$$

where c fixed the mean area at the starting time. As expected, $\alpha = 1$. A time or scale dependent diffusion constant (like that hypothesised for the soap froth, and observed in impure metals) leads to a variety of other growth laws.

V.d Topological Mean Field Theories

The simplest approach to a model which includes topological transformations as well as von Neumann's law, is to neglect spatial structure entirely and treat the system as homogeneous and completely described by its distribution functions. Hillert proposed a model basically of this type looking at the spread of topological charge as a series of defect climbs, but he did not develop the model to any great extent nor did he derive equilibrium distribution functions.[43,106]

Fig. 21 Elementary Topological Processes. (a) Side Swapping or $T1$ process. (b) Disappearance of a three-sided bubble or $T2(3)$ process. (c) Disappearance of a four-sided bubble or $T2(4)$ process. (d) Disappearance of a five-sided bubble or $T2(5)$ process. (e) Wall breakage next to an n-sided bubble, $Break(n)$. Numbers are keyed to Table 6.

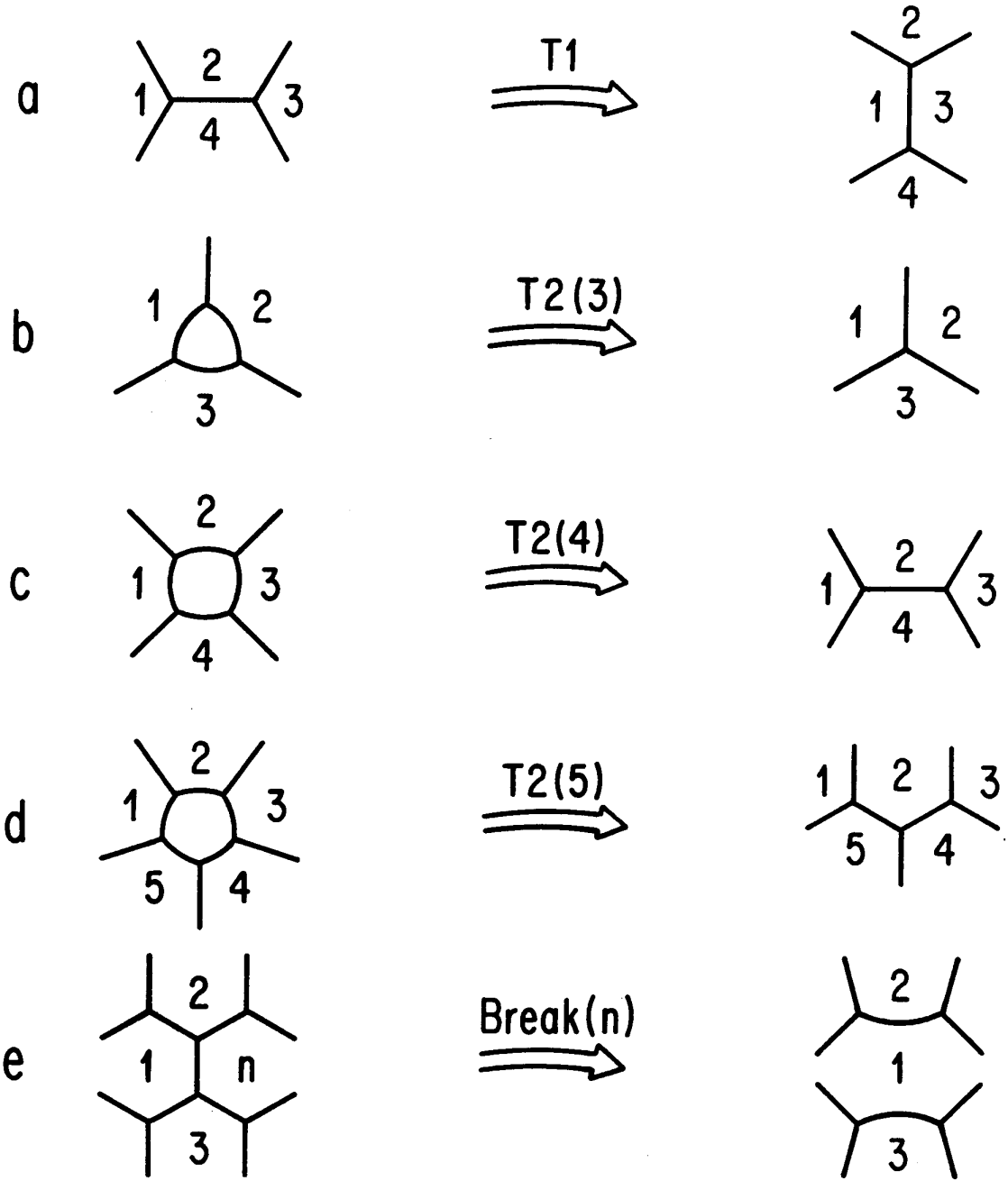
a
1
2
3
4
T1
2
1
3
4
b
1
2
3
T2(3)
1
2
3
c
2
1
3
4
T2(4)
1
2
3
4
d
2
1
3
5
4
T2(5)
1
2
3
5
4
e
2
1
n
3
Break(n)
2
1
3

TABLE 6

SCATTERING PROCESSES

Change	Bubble Number				
Process	1	2	3	4	5
T1	+1	−1	+1	−1	-
T2(3)	−1	−1	−1	-	-
T2(4)	−1	0	−1	0	-
T2(5)	−1	+1	−1	0	0
Break(n)	$+n-4$	−1	−1	-	-

Blanc, Carnal and Mocellin appear to have been the first to apply a topological mean field theory (they used only the number of side distribution) to grain growth.[30,46] We originally attempted such a mean field theory approach using separate distribution functions for the number of sides and areas with some qualitative but little quantitative success. This model was later refined by Marder who employed a joint probability distribution $\rho(n, A)$,[157] and by Beenakker.[26,27,28]

Any topological mean field theory for the soap froth starts with two basic components, the dynamics given by von Neumann's law, and a list of fundamental processes, scattering processes if you like, which describe the allowed changes in the distribution function. In general there can be an arbitrary number of different scattering processes, but all the possible behaviors of the soap froth can be described by five fundamental processes, of which only four enter into the models we will discuss.

When shear stresses are present in the froth, a pair of adjacent bubbles can be squeezed apart by another pair, as shown in Fig. 21 (a). This is known as a $T1$ process or **side swapping**. In this case the two bubbles that were neighbors each lose a side and the new adjacent bubbles each gain a side. Topological charge, $\mathcal{T} \equiv (n-6)$ is conserved since the total number of sides of the four bubbles before and after the swap is the same.

The disappearance of a bubble, a $T2$ process, also results in changes to its neighbors' number of sides. Topological charge is conserved in all disappearances so once again the results depend only on the number of sides

of the disappearing bubble. When a three-sided bubble disappears (Fig. 21 (b)) each of its neighbors loses a side. The equation for topological charge is $\mathcal{T} = -3 = 3 \times -1$. When a four-sided bubble disappears (Fig. 21 (c)) two of its neighbors stay the same and two lose a side. The equation for topological charge is $\mathcal{T} = -2 = 2 \times -1 + 2 \times 0$. Finally, when a five-sided bubble disappears (Fig. 21 (d)), one of its neighbors gains a side, two stay the same and two lose sides. The equation for topological charge is $\mathcal{T} = -1 = 1 \times 1 + 2 \times 0 + 2 \times -1$.

Wall breakage (Fig. 21 (e)) is only a slightly different problem. When a wall between an n-sided bubble and an m-sided bubble breaks, the resulting bubble has $n + m - 4$ sides and the two common neighbors each lose a side. Thus there is a total loss of 6 sides and 1 bubble, preserving topological charge. Note that wall breakage is the only mechanism that favors the creation of many-sided bubbles. The $T1$ process by itself is in equilibrium with a slowly decreasing $\rho(n)$ (See Table 7 under Fradkov ∞) and bubble disappearance results in exponential cutoff for large n. We may represent all these relationships conveniently in a table (Table 6) which encodes all the basic topological information about scattering in a connection number three lattice.

While the rates for disappearances of bubbles are fixed by the distribution functions and von Neumann's law, side swapping and wall breakage depend on different mechanisms and thus have rates independent of the basic froth evolution. Experimentally we observe little side swapping at long times since

the soap froth is soft and tends to eliminate stresses quickly and over short range. Some side swapping does occur, however, in the immediate vicinity of disappearing bubbles. Therefore some of the models discussed include side swapping as an external parameter. None of the models considers wall breakage, but that rate too could easily be included. One peculiarity of three dimensional models that examine two dimensional sections is that they must include the creation of three-sided grains caused by the growth of a previously unseen grain into the plane being examined.

V.d.i Pure Topological Theories

Blanc, Carnal and Mocellin have solved the equilibrium distribution function $\rho(n)$ subject to three scattering processes, side swapping, three-sided bubble disappearance and three-sided bubble creation.[30,46] The presence of three-sided bubble creation makes this model appropriate to three dimensions where three-sided bubbles can "nucleate" in a planar section as growing bubbles come to intersect the section. They require two parameters to specify their model, the proportion of three-sided bubbles $\rho(3)$, and the rate of side swapping. In their first paper they fixed the rate of three-sided bubble creation and adjusted the rate of side swapping to achieve a target $\rho(3)$. In their second paper they kept the rate of side swapping as a free parameter and adjusted the rate of three-sided bubble creation to achieve the target $\rho(3)$. The probability that a given $T1$ process affects an n-sided grain (n

restricted to be > 3) is just

$$\phi_n \equiv \frac{n\rho(n)}{6}. \tag{V.32}$$

The probability that a three-sided grain appears or disappears next to an n-sided grain is not *a priori* defined. They choose to use the value

$$\psi_n \equiv \frac{n^\gamma \rho(n)}{\sum_n n^\gamma \rho(n)}, \tag{V.33}$$

where γ is rather arbitrarily defined to be the solution to

$$\sum_{n=3}^{\infty} n^{\gamma+1}\rho(n) = \sum_{n=3}^{\infty} n^\gamma \rho(n) \left[7 + \frac{1}{3}\sum_{n=3}^{\infty}(n-6)^2\rho(n)\right]. \tag{V.34}$$

They then solved for the equilibrium of the system using montecarlo techniques. We present their results for no swapping and for a fixed rate of side swapping in Tables 7 and 8. The parameter β is approximately the reciprocal of the rate of $T1$'s.

Kurtz and Carpay, in a paper chiefly devoted to three dimensional grain growth considered a two dimensional topological mean field theory subject to von Neumann's Law.[132] They took the distribution of grain areas in each topological class to be a fixed log normal distribution,

$$\rho(r_n) = \frac{1}{(2\pi\sigma^2)^{1/2}}\frac{1}{r_n}\exp\left(-\frac{(\ln r_n - < r_n >)^2}{2\sigma^2}\right), \tag{V.35}$$

where $< r_n > \equiv c\ln(\frac{n}{<n>})$. This distribution is approximately correct for a two dimensional section of a three dimensional froth, but is not a very good description of a true two dimensional froth. They assumed everything else was random and solved by montecarlo as above. We present their results in Tables 7 and 8. They have also performed the entire calculation in three dimensions.

Fig. 22 Average Area versus Time. (A) For Marder's mean field theory (From Marder 1987).[157] (B) From Fradkov, Shvindlerman and Udler's network model (From Fradkov, Shvindlerman and Udler 1985).[261] (C) Average radius versus time for Beenakker's network model for ordered (O) and disordered (D) initial conditions (From Beenakker 1988).[262]

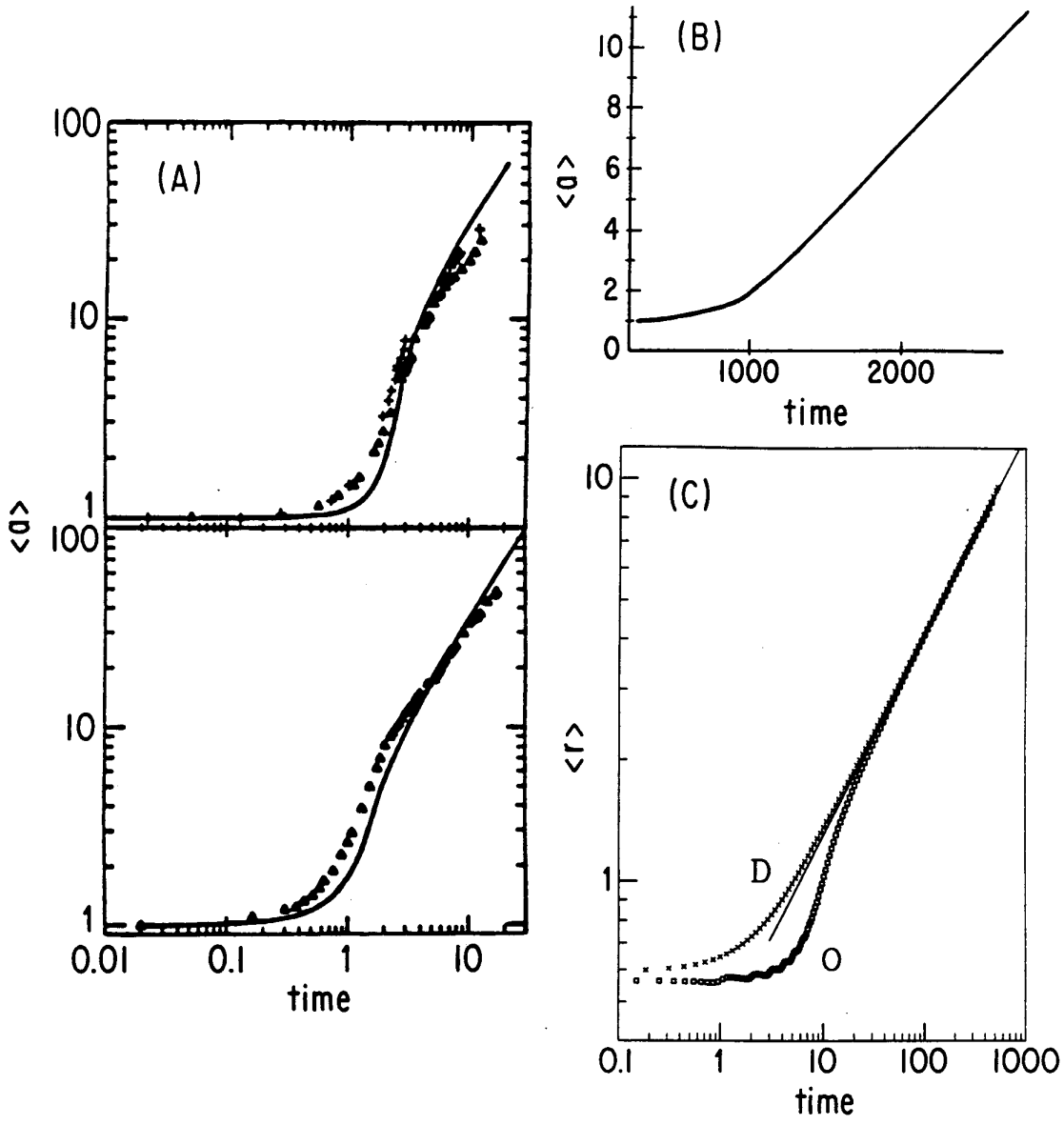
(A)
100
10
1
<D>
100
10
1
0.01
0.1
1
10
time
(B)
10
8
6
4
2
0
<D>
1000
2000
time
(C)
10
1
<r>
D
O
0.1
1
10
100
1000
time

V.d.ii A Complete Mean Field Theory

Marder attempted a true mean field theory depending only on the evolution of the distribution functions. He built his model as follows: Let $\rho(n, A, t)$ be the joint distribution function, and $g(n, A, t) \equiv N(t) * \rho(n, A, t)$. At any given time each n-sided bubbles obeys von Neumann's law, so it shifts the distribution per unit time as

$$\frac{dg(n, A)}{dt} = \frac{\partial A}{\partial t}\kappa(6 - n)g(n, A, t), \tag{V.36}$$

where the diffusion constant κ is now dimensionless. The change in number of bubbles with area A and n sides is now just the result of von Neumann's law plus the probability that a bubble with area A and $n+1$ sides loses a side or a bubble with area A and $n-1$ sides gains a side minus the probability that a bubble with area A and n sides either loses or gains a side, i.e.,

$$\begin{aligned} \frac{\partial}{\partial t}g(n, A) &= \frac{\partial}{\partial A}\kappa(6 - n)g(n, A, t) \\ &+u(A)\frac{n-1}{S}g(n-1, A) + d(A)\frac{n+1}{S}g(n+1, A) \\ &-[u(A) + d(A)]\frac{n}{S}g(n, A), \end{aligned} \tag{V.37}$$

where S is the total number of sides (a bubble with more sides is more likely to be chosen at random), $u(A)$ is the probability that a bubble of area A gains a side, and $d(A)$ is the probability that a bubble of area A loses a side.

Marder next assumed that the smallest bubbles neighboring a disappearing bubble tend to lose a side and the largest to gain a side. In this case

$$d(A) = d_5(A) + d_4(A) + d_3(A), \tag{V.38}$$

where:

$$d_5(A) \equiv \kappa g(5,0)5!(\frac{p^4(A)}{4!} + (1-p(A))\frac{p^3(A)}{3!}) \qquad \text{(V.39)}$$

is the probability to be next to a disappearing five-sided bubble and smallest or next smallest among the bubble's neighbors.

$$d_4(A) \equiv \kappa g(4,0)4!(\frac{p^3(A)}{3!} + (1-p(A))\frac{p^2(A)}{2!}) \qquad \text{(V.40)}$$

is the probability to be next to a disappearing four-sided bubble and smallest or next smallest among the bubble's neighbors.

$$d_3(A) \equiv \kappa g(3,0)3! \qquad \text{(V.41)}$$

is the probability to be next to a disappearing three-sided bubble. Similarly,

$$u(A) = \kappa g(5,0)5!\frac{[1-p(A)]^4}{4!} \qquad \text{(V.42)},$$

is the probability that a bubble is next to a disappearing five-sided bubble and is the largest. We present results from Marder's direct solution of the model in Table 7. Impressively for a model with no free parameters, Marder obtained quite good quantitative agreement with actual experimental time series for $< a(t) >$ (see Fig. 22 (A)), including the correct transient behavior for two different initially well ordered experimental runs.

If we assume that there is no correlation in side shedding we instead obtain

$$u(A) = \kappa g(5,0)5!\frac{2}{5} + g(4,0)4!\frac{2}{4} + g(3,0)3!\frac{3}{3} \qquad \text{(V.43)}$$

and

$$u(A) = \kappa g(5,0)5!\frac{1}{5}. \qquad \text{(V.44)}$$

This last is essentially a discretized version of the equations used in early work by Beenakker.[26] Fradkov has also taken this approach and solved for the equilibrium distributions retaining the rate of $T1$'s as a free parameter.[74]

V.e Evolution on a Network

Conceptually, the most satisfying approach to a mean field theory is that of the topological network. This was originally described by Fradkov, Shvindlerman and Udler, and apparently rediscovered independently by Beenakker[27,76] They model the froth as a connected network of bubbles where each bubble is completely described by its area, number of sides and list of neighbors. The mean field theory assumption is that side redistribution occurs randomly upon the disappearance of a bubble. The simulation is then straightforward. Von Neumann's law is applied to each bubble in the network, and the first time at which any bubble disappears, calculated. Next, the areas of all bubbles in the network are recalculated. The disappearing bubble is then deleted, its neighbors have their numbers of sides updated according to Table 6 and the list of neighbor connections is corrected according to Fig. 21. Almost any function of interest, $< a(t) >$, side and area distributions and correlations, etc., can be directly calculated from the state of the network as it evolves in time. The only aspect of the froth abandoned by the model is the deterministic redistribution of sides upon bubble disappearance. We may also include wall breakage processes without any detailed modifications.

Fradkov, Shvindlerman and Udler assumed direct disappearance of

three-, four- and five-sided bubbles with no redistribution correlations and included the rate of $T1$ processes as an adjustable parameter to obtain a family of side distributions.[76,77] For non-zero rates of side swapping they allowed the creation of two-sided bubbles. The greater the rate of T1's the lower the value of n at which the distribution peaked and the larger the value of $\rho(3)$ (See Table 7). They also observed the expected monotonic increase in growth rate to equilibrium for initially disordered states (See Fig. 22 (B)).

Beenakker employed the same model setting the rate of T1's to zero and assuming no redistribution correlations. He obtained excellent results for λ_n and the area distributions (See Table 7). Particularly striking was his observation of the characteristic features of both initially ordered growth (slow, fast, equilibrium) and initially disordered growth (monotonic increase to equilibrium rate), as well as the broadening and subsequent narrowing of the side distribution for initially well ordered distributions (See Fig. 22 (C)).

V.f "Exact Models"

As we shall see in the next chapter, mean field theories can predict well experimentally observed distribution functions. What they cannot do is generate an actual image of an evolving froth. To produce such a real space picture we must simulate the behavior of the froth directly as a combination of soap films and diffusing gas (or in the next section, as an array of hopping atoms). For want of a better term we call these "exact" models, though they are by no means always exact. "Exact" models come in two types. They either move the films and then adjust the vertex positions (boundary

dynamic models), or adjust the position of the vertices and then recalculate the positions of the soap films (vertex models). We begin by examining boundary dynamic models.

V.e.i Boundary Dynamic Models

Ceppi and Nasello[47,48] assumed a radius based dynamics, $v = \frac{\mu}{\rho}$, where v is the velocity of a given boundary, and ρ its averaged curvature. They then discretized to a lattice and defined the function

$$F_i(\vec{x}) \equiv \int_{C(\vec{x},a)} f_i(\vec{x}\prime) d\vec{x}\prime, \tag{V.45}$$

where $f_i(\vec{x})$ is one inside the ith bubble and zero outside, and $C(\vec{x},a)$ is a circle of radius a (in their paper, six lattice constants) centered at $\vec{x}$. The boundary between bubble i and bubble j was then given by solving implicitly for the position that yielded $F_i(\vec{x}) = F_j(\vec{x})$. They claimed that this evolution law was equivalent to the velocity relation with a time step of $\Delta t = a^2/6\mu$. Disappearing grains were eliminated from the list, and boundary reconnection was taken care of automatically by the definition. We show a typical example of the evolution they obtained in Fig. 23. Taking iterations of the algorithm as equivalent to time, they obtained $\alpha = 1$.

Frost, Thompson and their collaborators, in a long series of articles,[79,81,82,83,84,109,229] tried to duplicate the physical situation more realistically. They took equation (III.8):

$$\vec{v}(\vec{x}) = \mu(\vec{x}) \frac{\hat{n}(\vec{x})}{\rho(\vec{x})}, \tag{V.46}$$

as their basic dynamics, and discretized by segmenting the boundary into short, nearly flat sections represented by a point. The boundary segments were then moved perpendicular to the boundary a distance $v\Delta t$, to obey the dynamical law. Vertices were separately adjusted to give 120° angles, and radii of curvature calculated by local fitting of circular arcs. Boundary points were added or removed as needed to minimize errors in the curvature calculations. Side readjustments were made locally when vertices moved too close together. In spite of the numerous opportunities for error in the various discretizations, the model satisfied von Neumann's law to within 3%, convincing evidence that it captured the basic dynamics correctly.[80] It was straightforward to measure distribution functions and growth rates. We present a typical pattern evolution from their model in Fig. 24. Since the model stored only information describing the positions of boundaries they could run extremely large simulations, to obtain $\alpha = 1$ over three full decades for a variety of initial conditions. Unfortunately all of their initial conditions were fully disordered so they were not able to observe the disordering transient. One particularly attractive feature of this model is that it is simple to include a whole variety of evolution equations once the basic structure of the model has been established. Frost and Thompson have considered anomalous grain growth (by locally increasing the boundary mobility, μ), continuous nucleation of new grains, and non-linear curvature dependence among many other effects.

Fig. 23 Boundary Dynamic Grain Growth. (A) Initial Condition. (B) After 5 iterations of the algorithm. (C) After 20 iterations. (D) After 40 iterations (From Ceppi and Nasello 1984).[47]

A)

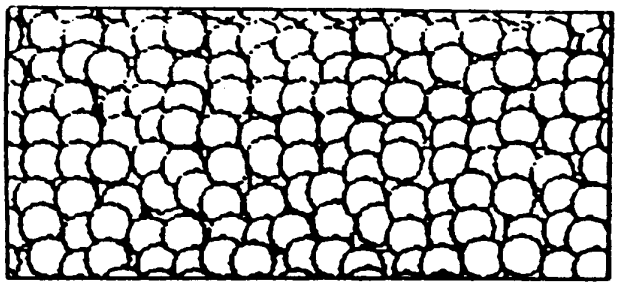

B)

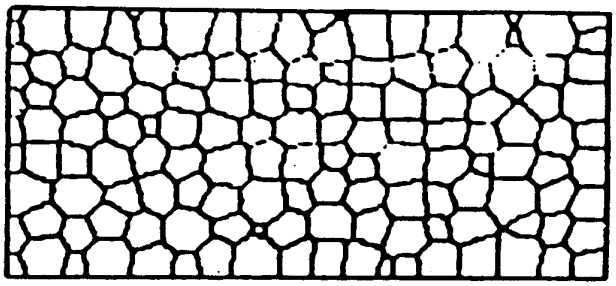

C)

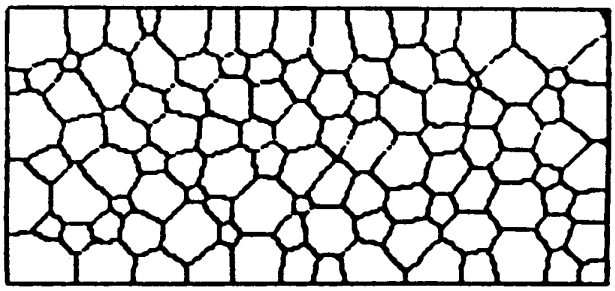

D)

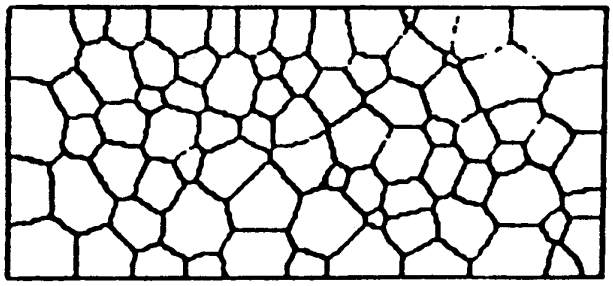

Fig. 24 Boundary Dynamic Grain Growth. Grain growth in the boundary dynamic model of Frost *et al.*. (A) Initial excluded volume Voronoi construction. (B) $t = 0.5$ diffusion times. (C) $t = 1.0$ diffusion times. (D) $t = 3.0$ diffusion times. (E) $t = 10.0$ diffusion times. (F) $t = 30.0$ diffusion times (From Frost and Thompson 1988).[260]

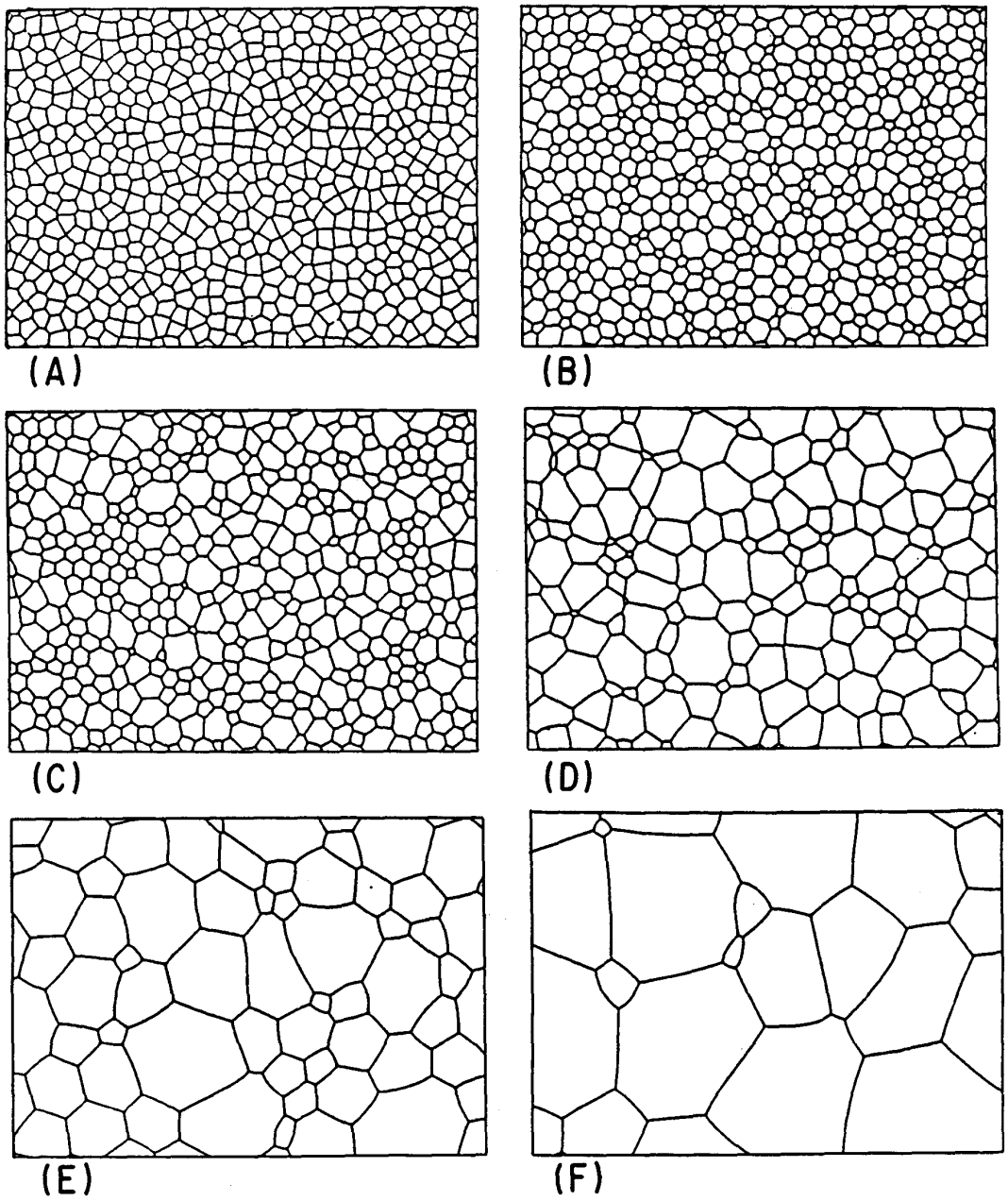
(A)
(B)
(C)
(D)
(E)
(F)

Fig. 25 Vertex Dynamic Grain Growth. Left hand side of each column shows the evolution of an experimental two dimensional soap froth, right hand side shows the evolution of a vertex model starting from identical initial conditions. (A) (left) $t = 990$ minutes. (A) (right) $t = 820$ minutes. (B) (left) $t = 1319$ minutes. (B) (right) $t = 1236$ minutes. (C) (left) $t = 1620$ minutes. (C) (right) $t = 1652$ minutes. (D) (left) $t = 2040$ minutes. (D) (right) $t = 2068$ minutes. (E) (left) $t = 2690$ minutes. (E) (right) $t = 2692$ minutes. (F) (left) $t = 3525$ minutes. (F) (right) $t = 3525$ minutes. Theoretical times were assigned by fitting $N(t = 0)$ and $N(t_{final})$ (From Fullman 1952).[86]

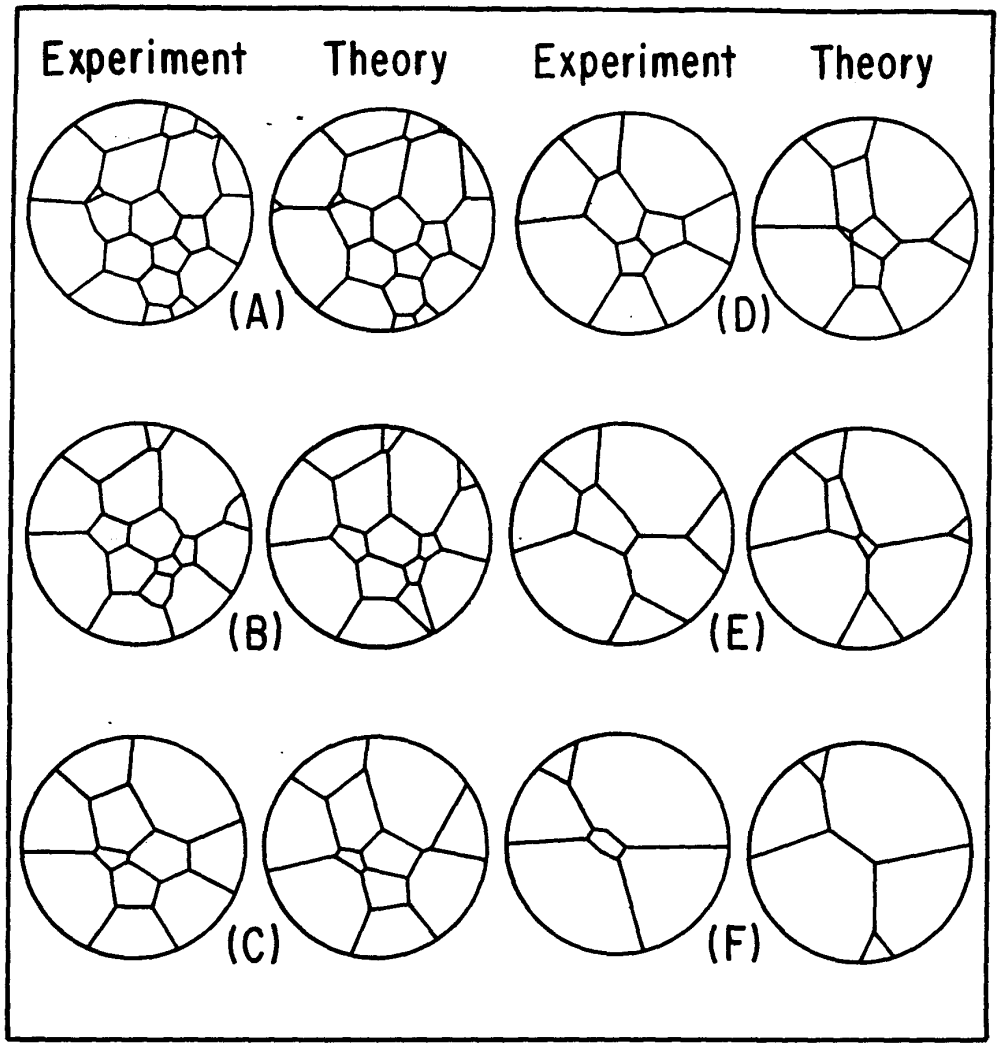
Experiment
Theory
Experiment
Theory
(A)
(D)
(B)
(E)
(C)
(F)

Fig. 26 Vertex Dynamic Grain Growth. (A) Voronoi network initial condition. (B) $t = 50$ time steps. (C) $t = 156$ time steps. (D) $t = 300$ time steps. (E) $t = 500$ time steps (From Soares, Ferro and Fortes, 1985).[210]

(A)

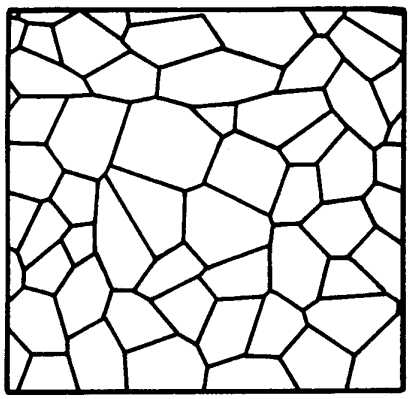

(B)

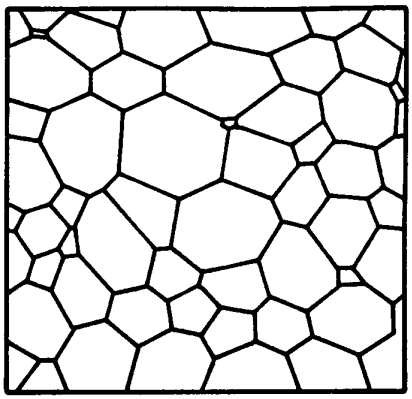

(C)

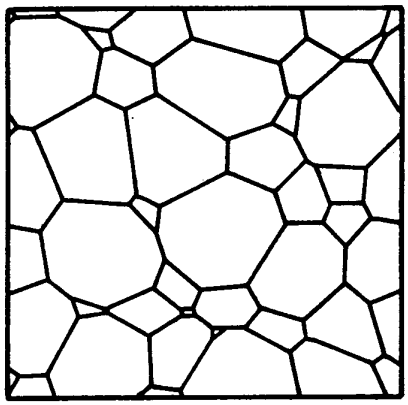

(D)

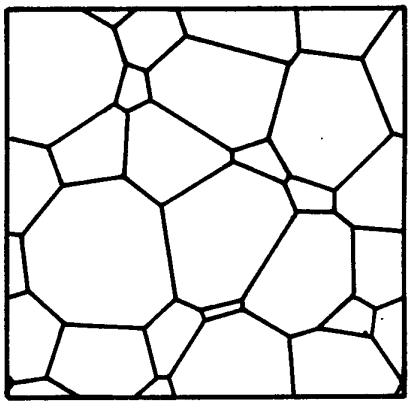

(E)

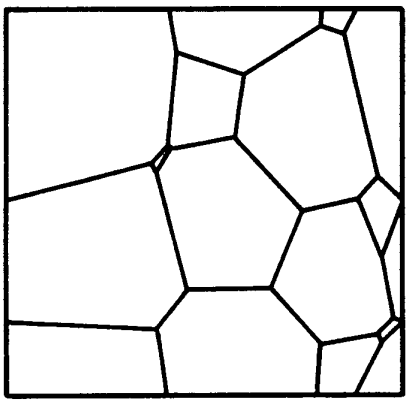

Fig. 27 Vertex Dynamic Grain Growth. Small samples of grain growth in the vertex model of Kawasaki, Nagai and Nakashima. They begin with a Voronoi lattice, $N = 48,000$. (A) $t = 5.0$ montecarlo steps (MCS). (B) $t = 20$ MCS. (C) $t = 50$ MCS (From Kawasaki, Nagai and Nakashima 1988).[259]

(A)

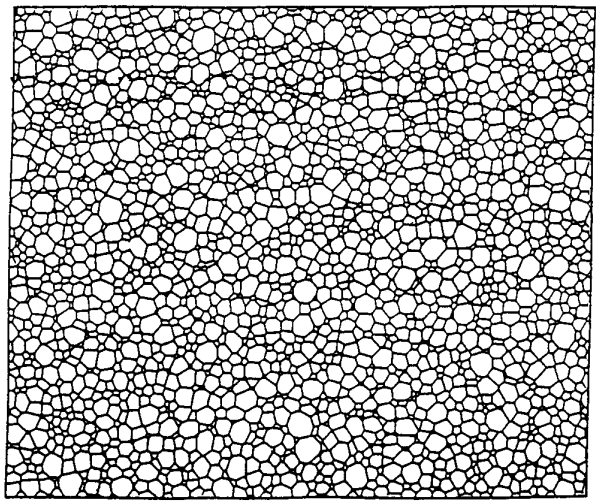

(B)

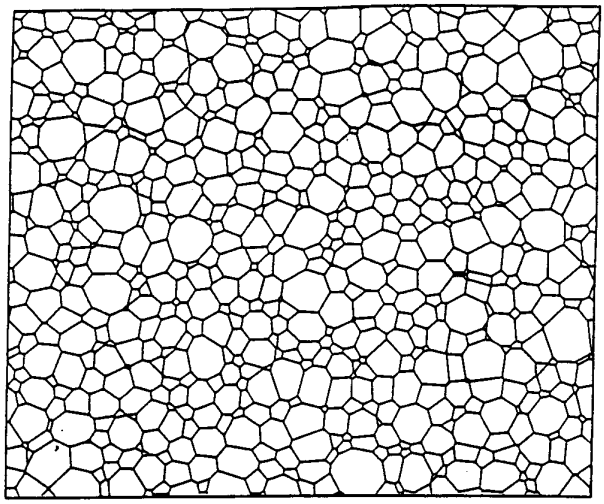

(C)

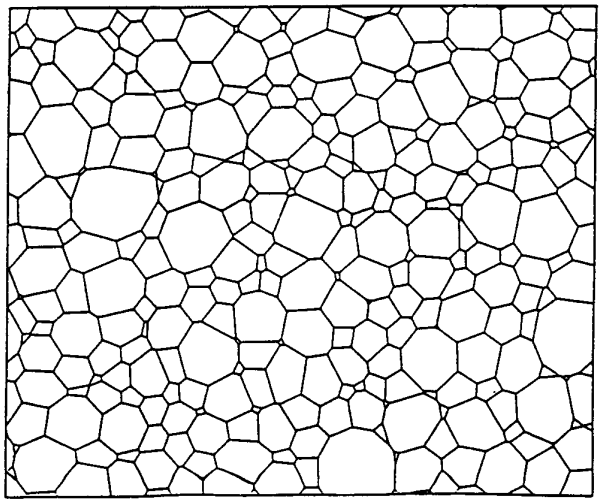

V.e.ii Vertex Dynamics

One appealing way to simplify the computation of bubble evolution is to treat the vertices as particles pulled by the grain boundaries. Such models have the advantage of extreme simplicity, but are not in any obvious way dependent on the real physics. We might expect them to work best in a different limit, when the diffusion rate across the grain boundaries was large compared to the rate of boundary motion. However, by choosing correctly the dependence of the vertex motion on applied force, we can obtain reasonable agreement with experiment.

The earliest example of a vertex model is that of Fullman (largely forgotten by later researchers).[86] He treated interfaces as flat and defined the force on a vertex j by

$$\vec{F}_i = \sum_{\substack{j=1,3 \\ neighbors}} \frac{\vec{x}_i - \vec{x}_j}{|\vec{x}_i - \vec{x}_j|}, \tag{V.47}$$

and the resulting velocity of the vertex by

$$\vec{v}_i = \vec{F}_i \frac{|\vec{F}_i|}{\sum_{\substack{j=1,3 \\ neighbors}} (\vec{x}_i - \vec{x}_j) \cdot \vec{F}_i} \tag{V.48}.$$

This effective mobility is a pretty good method to absorb an integrated wall curvature into an angle deviation at the vertex. Fullman did not discuss his treatment of bubble disappearance or side swapping (he did all his calculations by hand! which limited the number of bubbles he could work with), but it appears that he removed zero area bubbles directly, and swapped sides whenever vertex pairs overlapped. With this model, starting with an actual

soap bubble configuration, he was able to obtain good agreement both for the rate of area growth (Fig. 15 (B)) and for the detailed geometrical evolution of the froth (Fig. 25).

Soares, Ferro and Fortes also assumed that the froth behaves like a damped network of springs, and that pressure and diffusion could be neglected entirely.[210] That is, they assumed that wall mobilities were much greater than vertex mobilities. There is no reason *a priori* to expect that this should be true in the soap froth. They further assumed that boundary walls were flat, and the velocity of the ith vertex in the network given by

$$\vec{v}_i = \mu \vec{F}_i, \tag{V.49}$$

where μ is the mobility of the vertex, and F_i is the force on the vertex from equation (V.47). They performed side swaps whenever a given line connecting vertices shrank below a cutoff length l_0. Triangular cells with sides smaller than l_0 were deleted and replaced with a single vertex at the mid point of the triangle's shortest edge. As with all "exact" models, calculating distribution functions, etc. was straightforward. We show their sample evolution in Fig. 26, beginning with a Voronoi network and employing periodic boundary conditions. They obtained a value of $\alpha = 1.04$ for the area exponent.

Kawasaki, Nagai and Nakashima have developed a series of vertex based models that include a realistic description of the energetics of the soap films.[62,118,119,179] Instead of merely assuming a constant force dependent velocity, they included an explicit velocity dependent damping term. Let

$\vec{r}_i$ be the position of the ith vertex and σ be the surface tension. The free energy of the whole network then is :

$$\mathcal{F} \equiv \sigma \sum_{i,j} |\vec{r}_i - \vec{r}_j|. \tag{V.50}$$

If v_i is the velocity of the ith vertex and $\hat{n}_{ij} \equiv \frac{\vec{r}_i - \vec{r}_j}{|\vec{r}_i - \vec{r}_j|}$ is the normal between vertex i and vertex j, the dissipation is:

$$\mathcal{R} = \frac{\sigma}{6L} \left(\sum_i \sum_{\substack{j \\ neighbors(i)}} (\vec{v}_i \cdot \hat{n}_{ij})^2 + \sum_{\substack{i,\ j \\ (connected\ pairs)}} (\vec{v}_i \cdot \hat{n}_{ij})(\vec{v}_i \cdot \hat{n}_{ij}) \right), \tag{V.51}$$

where L sets the length scale of the pattern relative to the typical velocity. In terms of $\mathcal{F}$ and $\mathcal{R}$ the equation of motion for the ith vertex is given by:

$$\frac{\partial \mathcal{F}}{\partial \vec{r}_i} + \frac{\partial \mathcal{R}}{\partial \vec{v}_i} = 0. \tag{V.52}$$

These equations are not soluble for large numbers of bubbles. They may, however, be reduced to a soluble form by neglecting any anisotropy in the dissipation to obtain a simplified equation for the motion of a vertex

$$\frac{1}{6L} \sum_{\substack{j \\ neighbors(i)}} |\vec{r}_i - \vec{r}_j| \vec{v}_i = - \sum_{\substack{j \\ neighbors(i)}} \frac{\vec{r}_i - \vec{r}_j}{|\vec{r}_i - \vec{r}_j|}. \qquad \text{Model I (V.53)}$$

Averaging over the nearest neighbor lengths on the left hand side reduces the equation to an even simpler form:

$$\frac{1}{2L} \vec{v}_i = - \sum_{j,\ neighbors(i)} \frac{\vec{r}_i - \vec{r}_j}{|\vec{r}_i - \vec{r}_j|}, \qquad \text{Model II (V.54)}$$

equivalent to the model of Soares, Fero and Fortes. Kawasaki, Nagai and Nakashima treated swapping by setting any two vertices within a critical

distance to be equivalent, and replacing small triangles with a single vertex at the midpoint of the shortest side. They solved the equations by direct integration. We show the typical evolution of their Model II in Fig. 27 in a configuration beginning with a 48,000 bubble Voronoi lattice. The distributions were clearly much broader than in a real froth. Neither model obeyed von Neumann's law, with six-sided bubbles shrinking and few sided bubbles shrinking much slower than expected. In later papers they drew on the work of Fullman,[119] substituting the velocity dependence:

$$\vec{v}_i = \frac{\vec{F}_i \cdot \vec{v}_i / |\vec{v}_i|}{\sum_{\substack{j=1,3 \\ neighbors}} \frac{r_{ij}}{3L} \sin^2 \theta_{ij}}, \tag{V.55}$$

where θ_{ij} is the angle to the jth vertex. They also tried a local vertex mobility[62]

$$\mu_i \equiv \left(\frac{\sum_{\substack{j \\ neighbors(i)}} |\vec{r}_i - \vec{r}_j|}{6L} \right)^{-1}, \tag{V.56}$$

which gave more attractive distribution functions, with $\alpha = 1$, and obeyed both the Aboav-Weaire Law, and the radius law that $< r_n > \propto n$.

V.f.iii Other

Weaire and Kermode wrote a hybrid between a vertex and a boundary dynamic model.[243,244] They used von Neumann's law to adjust cell areas and then relaxed the positions of the vertices to produce 120° angles connected by minimal length circular arcs. They performed $T1$'s whenever vertex relaxation would have caused crossings in the boundaries and deleted very small three-, four-, and five-sided bubbles. They started their model with a

randomized lattice using periodic boundary conditions. Unfortunately limitations on the availability of computer time limited them to two hundred initial bubbles. Probably because of the small size of the simulation, they never seem to have reached a scaling state (their side distribution widened continuously), and they observed a growth exponent of $\alpha = 2$, typical of high growth rate equilibration. It is difficult to believe that they would not have obtained $\alpha = 1$ for a larger system. They did obtain good fits to experimental correlation functions and were able to perform a variety of rheological simulations.

V.g Potts Model

The vertex and boundary dynamic models we have been discussing arise naturally from a consideration of the basic physics of a soap froth, in which gas diffuses across well defined soap films. In a metal the grain boundaries are just regions of high concentrations of defects and move by the hopping of atoms between regions of different crystalline orientation. The Potts model simulation takes a quasi-microscopic view of froth evolution. It was developed by metallurgists who found it natural to think of the interior of a grain as being composed of a lattice of "atoms," and the grain boundaries, as the interface between different types (or orientations) of those "atoms." Philosophically this is as far as one can get from a mean field theory, but the starting point is not too different. The mean field theories begin with von Neumann's law, the Potts models with surface tension. The chief exponents of the Potts model approach have been the Exxon group of Anderson, Grest,

Sahni and Srolovitz who have published a monumental series of papers investigating every aspect of the model.[12,15,16,93,99,100,202,215,216,217,218,219]

We have mentioned in our discussion of von Neumann's Law that the basic driving force in a coarsening system is surface tension (or more generally surface energy) which creates pressure differences which result in gas diffusion. The Potts model puts surface tension on a lattice by defining an energy which is proportional to the total length of grain boundary in the system.

Mathematically we may do this by defining on each site of our lattice, a spin $\sigma_{(i,j)}$, where all the lattice points lying within a given grain in our initial configuration are assigned the same value of spin, with a different spin for each grain. In practice to increase computational efficiency, we may reuse spins, using a finite number Q of spins, but taking enough that the probability of two grains with like spins coming in contact and coalescing is small. will discuss below. The energy of interaction between like spins is defined to be zero, and between unlike spins to be one. We may thus write the total Hamiltonian for our spin system as:

$$\mathcal{H} = \sum_{i,j} \sum_{\substack{neighbors \\ i,j}} \delta_{\sigma(i,j),\sigma(i',j')} - 1, \qquad \text{(V.57)}$$

where the range of the second sum will affect the nature of the interaction. The spins are flipped using a montecarlo selection, where a spin is chosen at random and flipped only if the flip would lower system energy. This corresponds to the zero temperature limit, which is appropriate if we

Fig. 28 Potts Model Grain Boundary Migration. (A) Flat boundary, second nearest neighbor interaction. All boundary spins have energy 3, flips would increase energy to 5. (B) Curved boundary. Circled spins lose energy by flipping (6 → 3). The 2 grain will grow at the expense of the 1 grain.

A

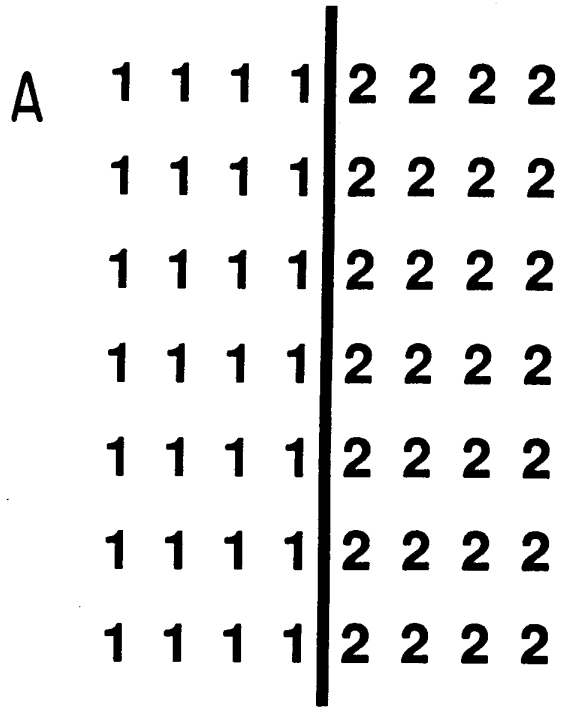
1 1 1 1 2 2 2 2
1 1 1 1 2 2 2 2
1 1 1 1 2 2 2 2
1 1 1 1 2 2 2 2
1 1 1 1 2 2 2 2
1 1 1 1 2 2 2 2
1 1 1 1 2 2 2 2

B

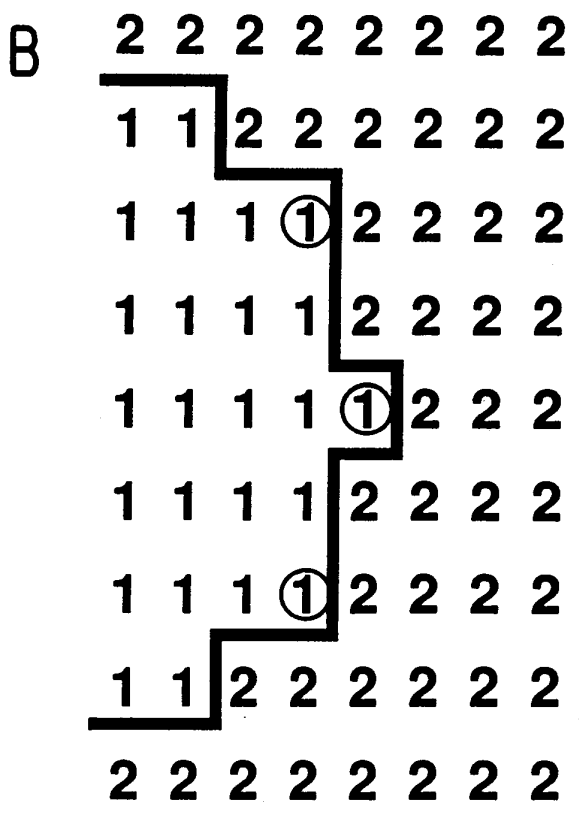
2 2 2 2 2 2 2 2
1 1 2 2 2 2 2 2
1 1 1 1 2 2 2 2
1 1 1 1 2 2 2 2
1 1 1 1 1 2 2 2
1 1 1 1 2 2 2 2
1 1 1 1 2 2 2 2
1 1 2 2 2 2 2 2
2 2 2 2 2 2 2 2

Fig. 29 Potts Model Anisotropies. Energy per unit surface length as a function of surface angle. (a) For nearest neighbor hexagonal lattice (From Srolovitz *et al.* 1983).[216] (b) For nearest neighbor square lattice. (c) For next nearest neighbor square lattice. Labelled arrows show energy extrema and values.

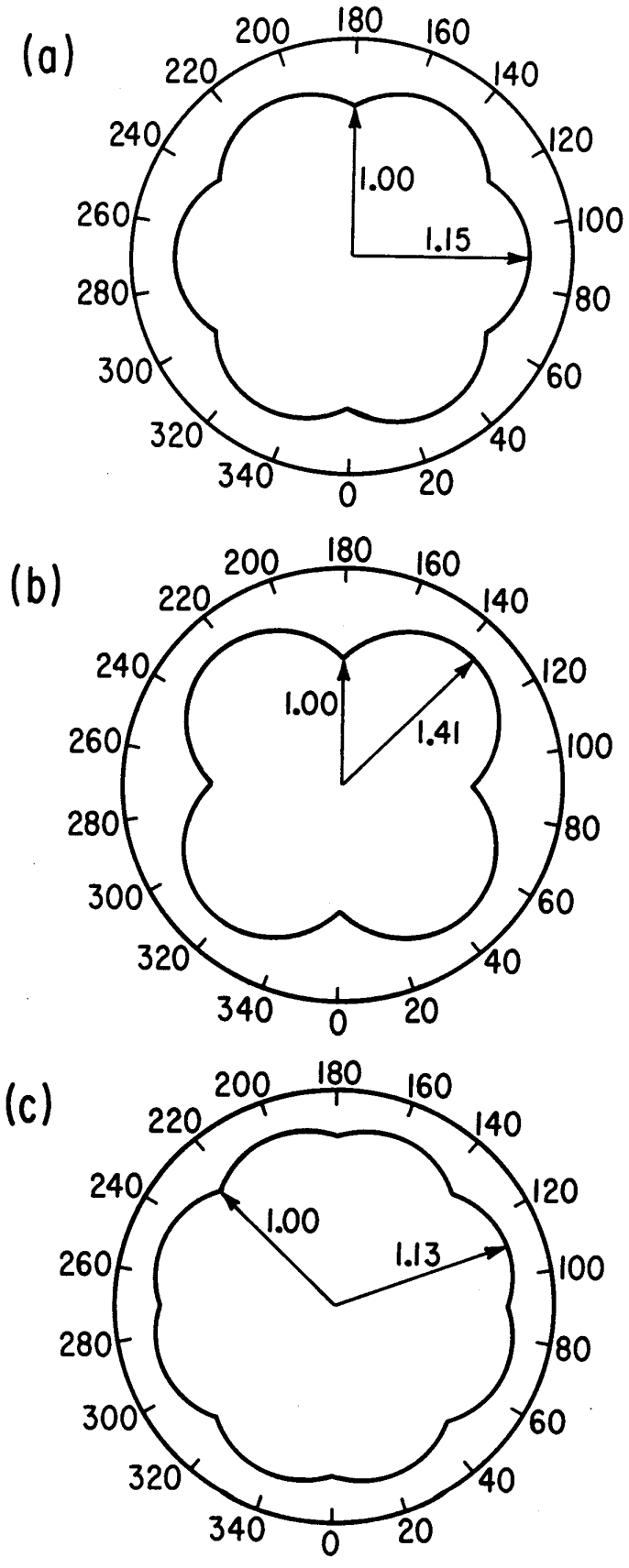
(a)
180
200
160
220
140
240
120
1.00
260
100
1.15
280
80
300
60
320
40
340
0
20
(b)
180
200
160
220
140
240
120
1.00
260
100
1.41
280
80
300
60
320
40
340
0
20
(c)
180
200
160
220
140
240
120
1.00
260
100
1.13
280
80
300
60
320
40
340
0
20

Fig. 30 Potts Model Anisotropy. Shrinking of an initially circular grain in an hexagonal nearest neighbor Potts model simulation. Times from outermost contour moving inwards are, $t = 0$, $t = 1200$, $t = 2100$, and $t = 3000$ montecarlo steps. Some hexagonal anisotropy is evident at later times (From Srolovitz *et al.* 1983).[216]

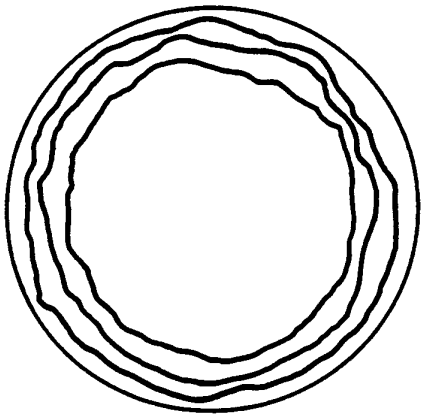

Fig. 31 Potts Model Grain Growth. Grain Growth in the next nearest neighbor $Q = 48$ Potts model starting with random initial conditions on a periodic lattice. (A) $t = 4,000$ montecarlo steps. (B) $t = 8,000$ montecarlo steps (C) $t = 12,000$ montecarlo steps. (D) $t = 20,000$ montecarlo steps (Figure supplied by G. S. Grest 1989).

(A)

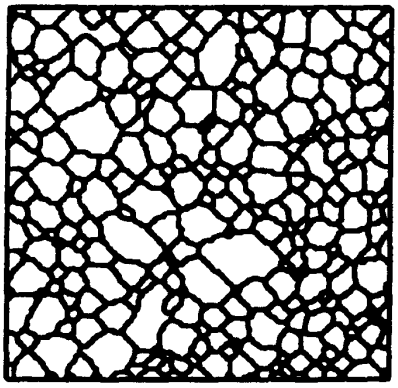

(B)

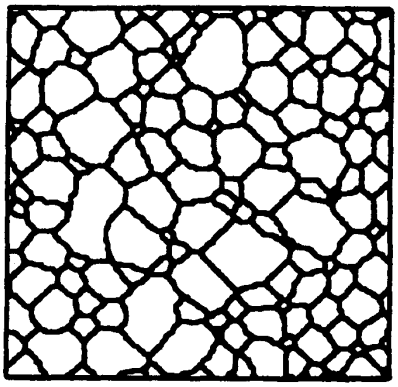

(C)

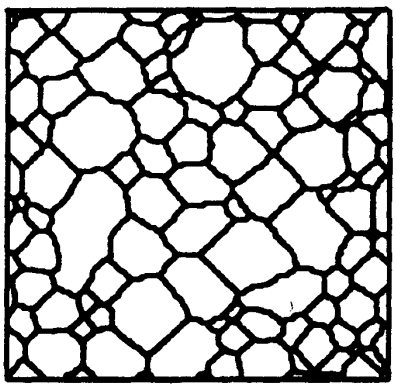

(D)

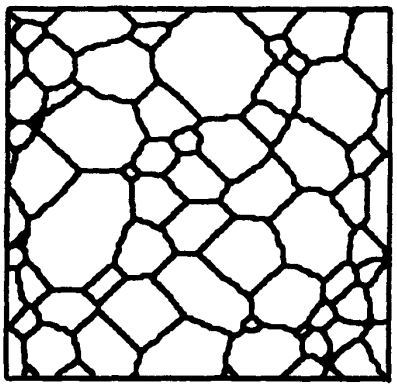

Fig. 32 Potts Model Grain Growth. Comparison of two dimensional soap froth (left) and next nearest neighbor square lattice Potts model simulation starting from identical initial conditions (right). Areas shown are 30% details of the soap froth and the entire 600 x 500 Potts model simulation. Note the missing walls along the lower boundary in the $t = 1640$ minute image and the spurious two-sided bubbles in the $t = 559$ minute and $t = 1119$ minute images (From Glazier *et al.* 1989).[93]

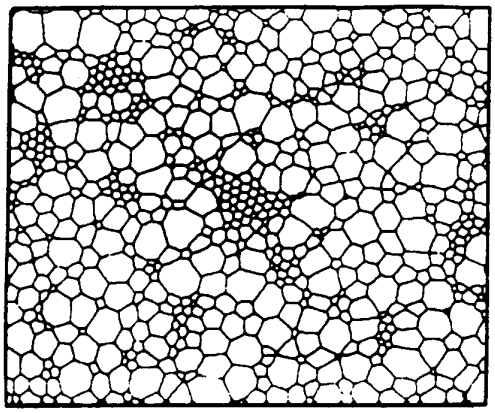

559 Minutes

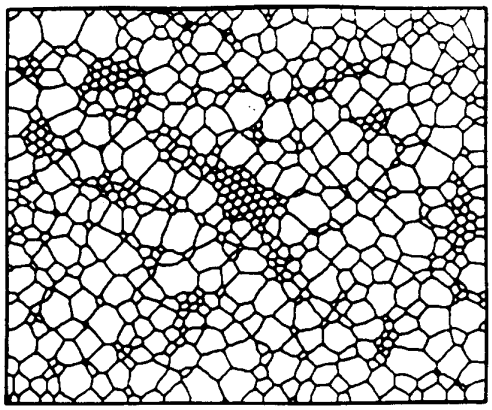

2000 MCS

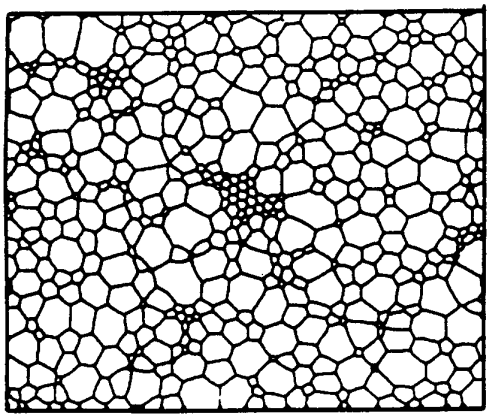

1119 Minutes

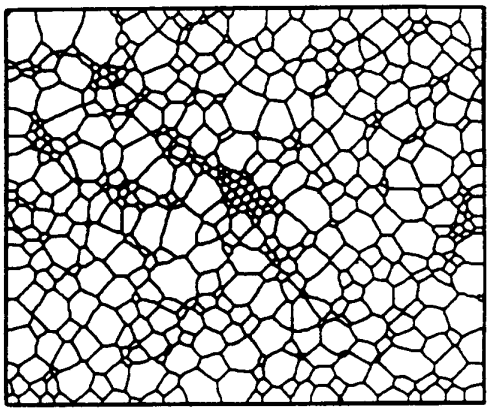

4000 MCS

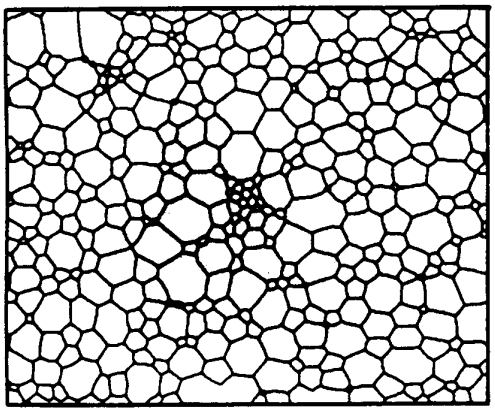

1640 Minutes

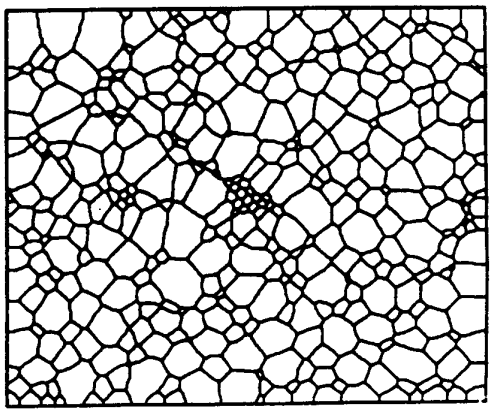

6000 MCS

want to study relaxation processes rather than phase transitions (The temperature remains a useful control parameter, however, for the analysis of conditions where fluctuations are significant).

We may understand why this surface energy results in a von Neumann like diffusion if we look closely at a region of grain boundary (Fig. 28). If the boundary is straight (Fig. 28 (A)) there is no tendency for spins to flip, since all spins border more of their own kind than of others. If a boundary is curved (Fig. 28 (B)), however, spins on the convex side will tend to see more of the opposing type and thus to flip. The result is that the boundary recedes at a rate proportional to its curvature. The original version of this argument was given by Plateau in his study of soap bubbles.[189,190] Since the system attempts to minimize surface length the same factors that favor 120° angles at vertices are at work, so the rest of the von Neumann's law derivation follows. One difficulty with this argument is that a simple nearest neighbor interaction on a square lattice results in a strongly anisotropic surface energy (the ratio of lowest to highest surface energies as a function of orientation is 1.41) which allows stable vertices deviating from the 120° rule (See Fig. 29 (b)). As a result grain growth in a nearest neighbor square lattice Potts model tends to gradually slow and finally stop altogether (as observed in many real metals with a high anisotropy), rather than coarsening continuously. One way to treat this problem is to work at a higher temperature where fluctuations overcome anisotropy pinning (experimentally in metals, higher temperatures result in larger growth exponents so this choice

is reasonable in simulations of grain growth). However, the soap froth is essentially fluctuation free, and therefore should be simulated in the zero temperature limit. A better solution is to use a nearest neighbor hexagonal lattice (Fig. 29 (a), energy ratio 1.15) or a next nearest neighbor square lattice (Fig. 29 (c), energy ratio 1.13), to reduce pinning. There is still some preferred boundary alignment in both cases, but no evidence of freezing. Anderson *et al.* have checked the anisotropy effect in the hexagonal lattice by tracking the evolution of an initially round grain (Fig. 30). It becomes slightly hexagonal, but continues to shrink essentially uniformly.

A second difficulty with the Potts model grain growth simulation is the range of length scales it requires. To successfully measure the scaling exponent for the growth of average grain area, for example, the following relation must hold:

$$L_{Lattice\ Spacing} << L_{Grain\ Initial} << L_{Grain\ Final} << L_{Lattice\ Size}, \tag{V.58}$$

i.e. each grain must contain many spins, the grains must grow a substantial amount, and the final configuration must have many grains. This means that for truly reliable results the lattice needs to be at least 1000 spins per side. An insufficient appreciation of this problem lead to some confusion over the actual scaling exponent of the model.[16,83] In their most recent paper the Exxon group obtained good agreement with von Neumann's Law. While they originally obtained a growth exponent of $\alpha = 0.76$ possibly due to non-equilibrium and anisotropy effects,[202] they have since revised their estimate

up to $\alpha = 0.98 \pm 0.04$.[15] In the same paper they obtained a growth exponent in three dimensions of $\alpha = 0.96 \pm 0.11$.

It is, perhaps, not too surprising that the Potts model shows excellent qualitative agreement with the coarsening of a soap froth. We show a simulated evolution of an initially random distribution of 48 different spin types ($Q = 48$) in Fig. 31.

In the case of the Potts model, we had the advantage of doing the simulations ourselves and could therefore match the conditions of the experiment and simulation more closely. We ran the simulation using a 600 x 500 square lattice with open boundary conditions (in which spins on the boundary were assumed to interact with frozen impurities) employing the digitized image at $t = 2044$ minutes as the initial state. As seen in Fig. 32, this time was late enough that there were few islands of six-sided bubbles remaining from the initial fill. We used a value of $Q = 48$ to minimize wall breakage without unreasonably increasing the time required for the computation. To prevent freezing of the domain boundaries at long times, we set the nearest and next nearest neighbor coupling constants equal. The resulting anisotropy appears as a preferential alignment of grain boundaries along 45° and 90° angles, which does not appear in the triangle lattice. However, grain areas and topological distribution functions appear to be independent of the lattice type, for simulations in which the boundaries do not freeze.

In Fig. 32 we show the soap froth (30% detail) and the Potts model at various stages of evolution, beginning with identical initial patterns. The

qualitative features of the disordering are similar, though the differing boundary conditions (the sample of the froth is taken from the bulk whereas the simulation has open boundary conditions) result in a rapid divergence between the actual patterns. A clear example of the difference in boundary conditions is the contact angle between the domain walls and the edges of the cell. In the experiment, the boundary of the viewing window does not affect the froth and the films can cross the boundary at an arbitrary angle. In the simulation (and adjacent to the cell walls in the experiment) the angle of contact is always close to 90°. The digitization can also result in the appearance of spurious small bubbles near the image boundaries and occasional wall breakage that they attempt to correct for in calculations. The disappearance of residual order occurs in both systems at comparable length scales (after approximately an one order of magnitude increase), and the qualitative patterns remain comparable. At long times in the Potts model grain boundaries appear to lie preferentially along 45° angles. This effect is not seen in simulations on the triangular lattice and presumably reflects the anisotropy remaining in the second nearest neighbor Hamiltonian.

In Fig. 17 we compare the average bubble size versus time for the froth and the model. Since the initial condition of the model was taken from the same digitized image used to measure the areas of the bubbles in the froth, there was no freedom in assigning areas to bubbles. The multiplicative constant relating real time to montecarlo steps is a free parameter, however. If we believe the result that the soap froth does show a growth in average area

slower than t at long times, we obtain from a least squares fit, t (minutes) $= t_m * .32 + 2044$, where t_m is the number of montecarlo steps. In this case we have essentially exact agreement between the froth and the model up to 20,000 minutes where the statistics are best, after which the rate of evolution of the soap froth slows noticeably. If we neglect the long term effect, we obtain a best fit with t (minutes) $= t_m * .38$, which gives agreement over the whole time period within approximately 20%. In both cases the typical dynamics for an initially ordered froth appear, slow initial evolution, followed by rapid growth during which any residual order disappears, and a long term tail with slower, approximately power law growth. We even obtain a purely fortuitous agreement in the long time tails of the two areas, where the soap froth and simulation both show non-monotonic changes in average area (at the same time) due to the contact with the cell boundary (and hence loss from the ensemble) of a large bubble.

Wejchert, Weaire and Kermode modeled the froth using a slightly different Potts model technique. They included von Neumann's law explicitly to control the dynamics in their calculations and used the hexagonal lattice Potts model only to relax the grain boundaries. They therefore used a different Hamiltonian,

$$\mathcal{H} = \frac{1}{2N} \sum_{i,j} \sum_{\substack{neighbors \\ i,j}} \delta_{\sigma_{(i,j)},\sigma_{(i',j')}} - 1 + \frac{\lambda}{N} \sum_{cells\ k} (a_k - \hat{a}_k)^2, \qquad \text{(V.59)}$$

where k indexes the bubbles, $\hat{a}_k$ is the von Neumann's law determined target area for the kth bubble, and λ specifies the strength of the area constraint. This Hamiltonian relaxes to the surface tension case with the constraint that

each bubble has a fixed target area $\hat{a}_k$. The target areas were updated according to von Neumann's law, $\frac{d\hat{a}_k}{dt} = \kappa(n_k - 6)$, at each time step. This had the advantage over the Exxon model that even bubbles small relative to the lattice constant properly obey von Neumann's law, since they are not dependent on statistical averaging along their walls, but the basic requirement of a large lattice remains.

The Potts model has several significant points in its favor. First is simplicity. Its one assumption is that wall energy is the only mechanism driving coarsening. Redistribution of sides occurs automatically without making further assumptions. $T1$ processes are also automatically included with the correct rate. Second, it can be easily extended to include grain coalescence and wall breakage. If, instead of assigning a different spin to each grain, a fixed number, Q, of spins are used, then the probability of a broken wall between two grains meeting as a result of a reorganization of the lattice is just $\frac{1}{Q}$. Thus one can study in detail the effects of wall breakage on froth evolution.[16,217] Other straightforward extensions include three dimensional lattices (limited by the availability of computer time to do 1000^3 monte-carlo calculations),[15] the consideration of pinning centers,[218] orientational anisotropies,[100] and anomalous grain growth in which volume dependent terms are added to the surface energy in the Hamiltonian.[219]

V.h Summary

We have examined seven basic types of models for coarsening in two dimensions: static models, phenomenological models, radius based mean

field theories, topological mean field and network models, boundary dynamic models, vertex dynamic models, and the Potts model. We draw the following conclusions about the physics of two dimensional coarsening. The phenomenological model's success shows that we understand the basic mechanism of disordering, that regions of homogeneous, unstable disorder eat away at regions of stable order along the boundaries between the regions. The ability of network models to reproduce the dependence of disordering on initial disorder confirms our basic statistical assumption, that the dynamics is independent of any correlations in side shedding. The ability of boundary dynamic models to predict both pattern evolution and dynamics goes a step further, demonstrating that local wall length minimization and the geometrical constraints of a coördination number three network can provide a complete description of two dimensional coarsening. Finally, the Potts model extends our understanding to the microscopic level, proving that purely local energy considerations at the "atomic" level can give rise to the correct diffusive and geometrical laws.

In this limited respect our understanding of the universal dynamics of two dimensional coarsening is complete. We have only hinted at the many types of non-universal behavior, which would be of paramount importance in any real application, because they are still poorly understood. We have also neglected three dimensional coarsening, another problem of great practical importance.